Received: June 15, 2020. Revised: August 12, 2020. 208

International Journal of
Intelligent Engineering & Systems

http://www.inass.org/

Detection of Microaneurysms Using Grey Wolf Optimization for Early Diagnosis of Diabetic Retinopathy

Manohar Pundikal[1]* **Mallikarjun Sayabanna Holi[2]**

[1]*Department of Electronics and Instrumentation Engineering, RNS Institute of Technology, India*
[2]*Department of Electronics and Instrumentation Engineering, University BDT College of Engineering, Davangere (A Constituent College of VTU, Belagavi), India*
* Corresponding author's Email: manoharasp@gmail.com

Abstract: The diabetic retinopathy is the leading cause of blindness worldwide, so early detection of diabetic retinopathy is necessary to reduce eye-related diseases. The accurate identification of microaneurysms is crucial for the detection of diabetic retinopathy, because it appears as the first sign of the disease. In this study, a new model is proposed to detect microaneurysms from the retinal images for early diagnosis of diabetic retinopathy. At first, the fundus images are collected from e-ophtha microaneurysms and DiaretDB1 datasets. Next, image pre-processing is accomplished using image normalization, low light image enhancement, gradient weighting and shade correction. The pre-processing methods significantly brighten the contrast of the fundus images for better visual quality and extract the hidden details of the dark conditions. In addition, Hessian based filter and Otsu threshold are used to extract the foreground objects like microaneurysms from the enhanced fundus images. At last, Grey Wolf Optimization (GWO) is used to predict the correctness of segmented microaneurysms candidates. The experimental results have revealed that the proposed model enhanced the microaneurysms detection up to 0.06-0.30 f-score value compared to the other existing models local convergence index features and local features with k-nearest neighbor. In addition, the proposed model has achieved 85.72% and 86.16% of accuracy respectively on e-ophtha microaneurysms and DiaretDB1 datasets.

Keywords: Diabetic Retinopathy, Grey wolf optimization, Hessian based filter, Microaneurysms detection, Otsu thresholding.

1. Introduction

In recent years, diabetic retinopathy becomes a serious eye disease that originates from diabetes mellitus and it is the most common cause of blindness in the developing countries [1]. The retinopathy is a thin layer of light sensitive tissues that lines the back of the eye. The retinopathy occurs due to the long standing of diabetes mellitus and as a result the blood vessels become leaky, blocked, and grow haphazardly [2]. The primary sign of diabetic retinopathy is microaneurysms that are a round intra retinal lesion ranging from 10 to 100 lm in size and red in color [3]. So, the detection of microaneurysms is crucial in preventing further progression of diabetic retinopathy [4]. The detection of microaneurysms depends on the characteristics of the imaging device and other image properties like type of compression. Some microaneurysms are easily spotted in the background of the retina, while identification of others is more difficult. Apart from the image characteristics, the spatial location also influences on the detection of microaneurysms; for instance, proximity of vessel parts [5]. Some of the previous methods used in microaneurysms detection are Multilayered thresholding based segmentation [6], circular Hough transformation [7], multi-scale Gaussian correlation filtering [8], Multi tolerance thresholding methodology [9], convolution neural network [10], etc. The subjective evaluation of fundus image leads to poor therapeutic choice that results in high mortality rate.

In this study, a new model is proposed to improve the performance of microaneurysms recognition. At first, the input fundus images are acquired from e-

ophtha microaneurysms and DiaretDB1 datasets. After collecting the retinal funds images, denoising is accomplished using normalization, low light image enhancement, gradient weighting and shade correction. The normalization and low light image enhancement techniques maintain the range of pixel intensity values that increases the visual quality of the retinal fundus image. Meanwhile, the small intensity variations in the green plane image background are removed in the pre-processing step, where the resultant image is named as "shade corrected" image. This image is generated by subtracting the background image from the green image. After pre-processing the images, the vessel is removed using Hessian based filter and Otsu thresholding with morphological operator. These methods were also used to segment and separate the overlapped non microaneurysms and microaneurysms candidates. At last, Grey Wolf Optimization (GWO) is used to predict the correctness of segmented microaneurysms candidates. In the result and discussion section, the performance of the proposed and existing work is discussed in terms of sensitivity against False Positive per Image (FPI), Area under Curve (AUC), f-score, and accuracy.

This research paper is prepared as follows: The Section 2 presents a survey on microaneurysms detection for the early diagnosis of diabetic retinopathy. A detailed description about the proposed model is presented in the Section 3. The experimental results of the proposed model are discussed in the Section 4. The conclusion of this study is drawn in the Section 5.

2. Literature survey

Selçuk and Alkan [11] developed an optimization algorithm to segment microaneurysms for the early recognition of diabetic retinopathy. Initially, the retinal structure was extracted from the fundus images, which were taken from DiaretDB1 and messidor datasets. Then, ant colony algorithm was used to segment microaneurysms from the collected retinal fundus images. The proposed optimization algorithm was compared with some existing clustering methods like region growing, k-means, random walker, watershed and maximum entropy to compare the effectiveness of the developed an algorithm with the existing methods. The simulation results indicated that the developed algorithm achieved better results compared to the existing methods in terms of Jaccard and dice coefficients. However, the optimization algorithm alone can't segment an image, because it requires a maximization or the minimization function to perform segmentation.

Xu, Zhang, Chen, Li, Zhang, Shao and Wang [12] developed a new automated framework to classify microaneurysms based on the longitudinal pathological factors. In this study, Support Vector Machine (SVM) was used to classify microaneurysms turnover by determining the variance of pathological risk factors for every episode. Next, the weight of each pathological risk factor was predicted that leads to microaneurysms turnover. The experimental analysis was performed on the Grampian diabetes database. The simulation outcome revealed that the developed framework attained better results compared to the prior research works in terms of specificity and sensitivity. However, the SVM classifier supports only binary classification, so it is difficult to classify the stages of disease.

Dashtbozorg, Zhang, Huang and Haar Romeny [13] presented a reliable and a new automatic system to detect the microaneurysms in the retinal images. Initially, an iterative thresholding technique and gradient weighting approach were used to extract preliminary microaneurysms candidates. Next, shape and intensity descriptors in terms of local convergence index filter were used to extract the features from each microaneurysms candidate. At last, a hybrid boosting and sampling classifier were used to classify the non-microaneurysms candidates and microaneurysms candidates. In this study, the developed system was validated based on the five online databases like DiaretDB1, e-ophtha microaneurysms, Retinopathy Online Challenge (ROC) and two Retina Check datasets. The experimental results showed that the developed system achieved better performance compared to the prior research works. However, in this study the semantic space between the extracted shape and intensity features was high that leads to poor classification.

Wu, Zhu, Shi, Zhu and Chen [14] presented a new system for the automatic detection of microaneurysms from the fundus images. The developed system had four major phases image collection, image denoising, candidate and feature extraction and classification. Initially, the fundus images were acquired from e-ophtha microaneurysms and ROC datasets. Then, illumination equalization and contrast limited adaptive histogram equalization were applied to those fundus images to improve the quality of the images. In candidate and feature extraction phase, region growing, peak detection, 27 profiles and local features were used to extract the features' values. These features were classified using k-nearest

neighbour classifier that distinguished both the non-microaneurysms and microaneurysms candidates. However, the dimension of the extracted features increase because of using a number of feature extraction techniques that may lead to poor classification.

Rosas-Romero, Martínez-Carballido, Hernández-Capistrán, and Uribe-Valencia [15] developed a new automated system for the early identification of microaneurysms from the fundus images. Initially, normalization and bottom hat transform were used to enhance the grayscale content and to eliminate the reddish regions that suppressed bright objects. Then, Principal Component Analysis (PCA) was used to extract the discriminant features from the denoised images. At last, a hierarchical classifier was implemented to distinguish the false positive and real microaneurysms based on the isolated blood vessel regions. In this study, the developed system's performance was validated based on the two databases E-ophtha microaneurysms and ROC. The simulation results indicated that the developed system achieved better classification performance compared to the existing methodologies. However, the hierarchical based classification approaches usually require huge volumes of data to achieve better accuracy that is a major drawback of this data information study.

Usman and Almejalli [19] presented a technique for automatic detection of microaneurysms from the fundus images. Initially, green channel was extracted and then median filtering was employed for removing random noise. Contrast limited adaptive histogram was to make certain areas more visible. In addition, shade correction and Gaussian filter were applied for enhancing the image contrast. Twenty-eight features were used to exploit the hidden dependencies among the features. Finally, binearization was used as fitness scores for image classification. In this literature, the dimension of the extracted features was high, which leads to curse of dimensionality concern.

S.B. Patil and B.P. Patil [20] presented a new method for microaneurysms detection on the basis of high boost filter, line detector and single class SVM. Initially, illumination equalization was applied for noise removal and then modified high boost filter was used for objects enhancement like blood vessels and microaneurysms. In this literature, region, geometric and intensity descriptors were used for extracting the features and then the extracted features were fed to single class SVM for classification. The single class SVM supports only binary class, where it was not applicable in multi class classification.

P. Chudzik, S. Majumdar, F. Calivá, B. Al-Diri and A. Hunter [1] developed a new patch based Fully Convolutional Neural Network (FCNN) model for the detection of microaneurysms. The developed model uses batch normalization and dice coefficient loss function to segment and detect microaneurysms. From the experimental analysis, the developed model attained better performance in microaneurysms detection. Usually, the deep learning network needs larger data to achieve better performance and also it was computationally expensive.

S. Long, J. Chen, A. Hu, H. Liu, Z. Chen and D. Zheng [21] used Directional Local Contrast (DLC) algorithm for detecting the microaneurysms. Initially, the blood vessel components were enhanced and segmented by Eigen values of Hessian matrix. Then, eliminate the blood vessels from microaneurysms regions by using connected component analysis and shape characteristics. After segmenting the patches, microaneurysms features were extracted and every candidate patches were classified as microaneurysm and non-microaneurysm candidates. The developed DLC algorithm was high dimensional in nature that leads poor classification performance.

This literature survey describes, enumerate, objectively evaluate, summarize and clarify the previous research works. This survey gives a

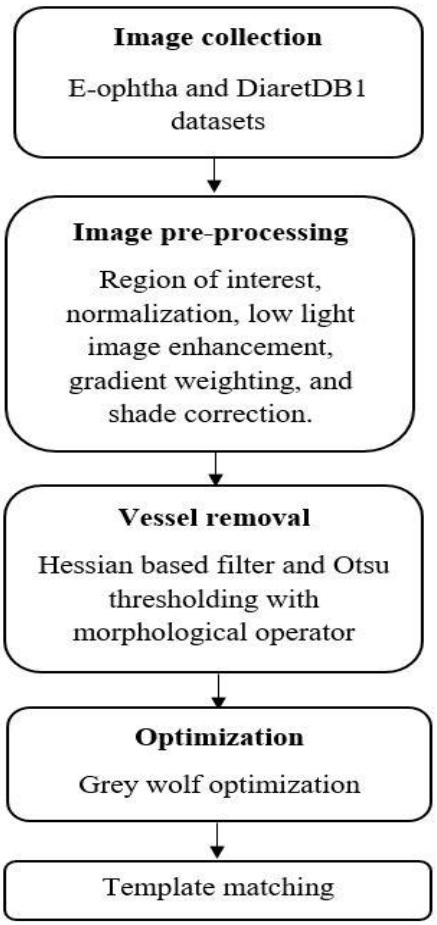

Figure. 1 Work flow of the proposed model

theoretical base to the researchers and assists them to determine the nature of the research. In this research paper, a new model is proposed to enhance the accuracy of microaneurysms prediction.

3. Proposed model

In the developing countries, diabetic retinopathy is one of the main reason of blindness if it is not recognized and treated in time. So, the early diagnosis of diabetic retinopathy is necessary to protect the person's vision. Reliable detection of microaneurysms is very necessary for the early detection of diabetic retinopathy, because it appears as the first sign of disease. In this study, a three stage model is proposed for the early detection data information of microaneurysms. In the first stage, image pre-processing is accomplished using normalization, low light image enhancement, gradient weighting and shade correction.

In the second stage, blood vessel removal is done by Hessian based filter and Otsu thresholding with morphological operator. At last, GWO is used to eliminate the non-microaneurysms regions from the images. Fig. 1 presents the work flow of the proposed model.

3.1 Dataset description

At first, the retinal fundus images are collected from E-ophtha and DiaretDB1 datasets. The E-ophtha database includes two sub datasets named as e-ophtha exudates, and e-ophtha microaneurysms [16]. In this research study, e-ophtha microaneurysms dataset is undertaken for microaneurysms detection that comprises of 233 healthy controls images and 148 images of small hemorrhages or microaneurysms patients. These images are acquired from four dissimilar image resolutions that ranges from 1440×960 to 2544×1696 pixels with 45^0 field of view. The sample collected microaneurysms image is graphically presented in Fig. 2.

Correspondingly, the DiaretDB1 is a public database, which is used to evaluate diabetic retinopathy detection models. The database contains digital images of eye fundus and expert annotated ground truth for several well-known diabetic fundus lesions (hard exudates, soft exudates, microaneurysms and hemorrhages) [13]. The original image of DiaretDB1 is presented in Fig. 3.

3.2 Image pre-processing

After collecting the retinal images, image pre-processing is accomplished using Region of Interest

Figure. 2 Sample collected images of E-ophtha dataset

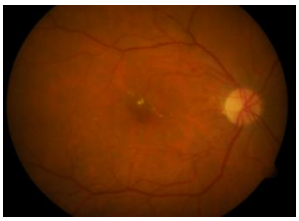

Figure. 3 Sample collected images of DiaretDB1 dataset

(ROI), image normalization, low light image enhancement, gradient weighting and shade correction. The ROI is defined as a subset of retinal fundus image or a database identified for blood vessel segmentation. Then, normalization is applied to alter pixel intensity values of the image to improve the quality of acquired fundus images by reducing the machinery and impulse noises from the images. Next, the deformations and alternations occurred in the fundus images due to imprecise image capture are identified. During image normalization, the acquired image is converted into pre-determined variables. The formula to estimate image normalization is mathematically denoted in Eq. (1).

$$IN = (I - Min) \times \frac{newMax - newMin}{Max - Min} + newMin \quad (1)$$

where, I is represented as input fundus image, IN is indicated as normalized image, $newMax - newMin$ is stated as intensity range of normalized image, and $Min = 0, and\ Max = 255$ is indicated as pixel intensity range of input image.

Similarly, low light enhancement and gradient weighting are used to brighten and improve the contrast of the fundus image for better visual quality and to extract the hidden details inform the image in dark conditions [17]. In order to correct the non-uniform illumination of the green channel fundus

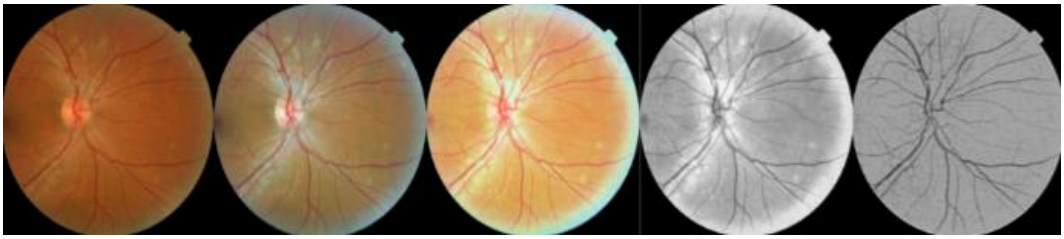

(a) (b) (c) (d) (e)

Figure. 4 Pre-processed image: (a) ROI image, (b) normalized image, (c) low light enhanced image, (d) gradient weighting, and (e) shade correction

image, it is first filtered (mask $=35*35$) to get the background image, then the background image is subtracted from the filtered image [18].The resultant difference image is a totally dark image, so it is easy to see any structures in the fundus images. The pre-processed image is graphically presented in the Fig. 4.

3.3 Vessel removal

The blood vessel removal is performed using Hessian based filter and Otsu thresholding approach after enhancing the image quality. The Hessian based filter is used to enhance the blood vessel structures by combining Hessian matrix with Gaussian convolution to tune the filtering response of the specific scales. Otsu threshold automatically threshold the grey image to a binary image that helps in extracting the foreground objects like blood vessels from the enhanced image. A detailed explanation about the undertaken approaches is discussed in the following section.

3.3.1. Hessian based filter

The Hessian based filter is used to enhance quality of the retinal fundus image that works based on the Hessian matrix. The eigenvectors and eigenvalue of Hessian matrix are closely related to the vascular direction and intensity. For a retinal fundus image I, Hessian matrix (3×3 matrix) is composed using second order partial derivatives that is mathematically presented in Eq. (2).

$$\nabla^2 I = \begin{bmatrix} \frac{\partial^2 I}{\partial x^2} & \frac{\partial^2 I}{\partial x \partial y} & \frac{\partial^2 I}{\partial x \partial z} \\ \frac{\partial^2 I}{\partial y \partial x} & \frac{\partial^2 I}{\partial y^2} & \frac{\partial^2 I}{\partial y \partial z} \\ \frac{\partial^2 I}{\partial z \partial x} & \frac{\partial^2 I}{\partial z \partial y} & \frac{\partial^2 I}{\partial z^2} \end{bmatrix} \quad (2)$$

At a point (x, y, z), the second order derivative of denoised fundus image I is determined as a convolution with derivative of Gaussian filter at a scale σ, which is mathematically presented in the Eqs. (3) and (4).

$$I(x, y, z, \sigma) = G(x, y, z, \sigma) \times I(x, y, z) \quad (3)$$

$$G(x, y, z, \sigma) = \frac{1}{\sqrt{(2\pi\sigma^2)^3}} \exp\left(-\frac{x^2+y^2+z^2}{2\sigma^2}\right) \quad (4)$$

Where, $G(x, y, z, \sigma)$ is denoted as Gaussian convolution kernel. Let, the eigenvectors of $\nabla^2 I$ are e_1, e_2, and e_3 and their corresponding eigenvalues are $\lambda_1, \lambda_1, and\ \lambda_3$ based on the $\nabla^2 I$ eigenvalues, the dissimilarity metrics R_B and R_A are calculated based on the Eqs. (5) and (6).

$$R_A = \frac{|\lambda_2|}{|\lambda_3|} \quad (5)$$

$$R_B = \frac{|\lambda_1|}{\sqrt{|\lambda_2 \lambda_3|}} \quad (6)$$

The first ratio R_A is used to distinguish the line and plate like structures and the second ratio R_B accounts for the deviation of blob like structure, so it cannot able to differentiate the line and plate like structures. In this scenario, frobenius norm is included in the Hessian matrix decrease the response of the background pixels that is theoretically named as "second order structure" which is mathematically presented in Eq. (7).

$$S = \sqrt{\lambda_1^2 + \lambda_2^2 + \lambda_3^2} \quad (7)$$

Then, the vesseleness function is determined by assuming a bright image that is formulated in Eq. (8).

$$\gamma_0(\sigma) = \begin{cases} 0, if\ \lambda_2 > 0 \text{ or } \lambda_3 > 0 \\ \left(1 - \exp\left(-\frac{R_A^2}{2\alpha^2}\right)\right) \exp\left(-\frac{R_B^2}{2\beta^2}\right) \\ \times \left(1 - \exp\left(-\frac{S^2}{2c^2}\right)\right), otherwise \end{cases} \quad (8)$$

Where, $\alpha, \beta,$ and c are denoted as threshold values that controls the sensitivity to measure R_A, R_B, and S. The maximum response is chosen as a final estimate of vesselness, as presented in Eq. (9).

$$\gamma_I = \max_{\sigma_{min} \le \sigma \le \sigma_{max}} \{\gamma_0(\sigma)\} \quad (9)$$

Where, σ_{max} and σ_{min} are denoted as maximum and minimum scales respectively that helps to identify the relevant structure. The maximum response output γ_I is the enhanced fundus retinal image that corresponds to line like structures. For 2D image, following vesselness measure is applied, as mentioned in Eq. (10).

$$\gamma_0(\sigma) = \begin{cases} 0, if\ \lambda_2 > 0 \\ \exp\left(-\frac{R_B^2}{2\beta^2}\right)\left(1 - \exp\left(-\frac{S^2}{2c^2}\right)\right), \\ otherwise \end{cases} \quad (10)$$

3.3.2. Otsu thresholding with morphological operator

Thresholding is the process of converting enhanced fundus images into bi-level images by applying an optimal threshold value, which helps to represent the image objects effectively in maps and graphs. The Otsu thresholding usually depends on discriminate analysis to find the maximum separability of class (non microaneurysms and microaneurysms candidates) and it minimizes the overlapping of class distributions. The Otsu thresholding approach segments the fundus image into two regions (light $T0$ and dark $T1$ regions), which are mathematically denoted in the Eqs. (11) and (12).

$$T0 = \{0,1, \dots., t\} \quad (11)$$

$$T1 = \{t, t+1, \dots., l-1, l\} \quad (12)$$

Where, t is represented as a threshold value and the maximum gray level value is one. The Otsu thresholding approach calculates all the possible values and estimates the minimum image pixel value of the threshold. The main objective is to identify the threshold value with less entropy based on the statistical information on the segmented fundus image. The optimal threshold value t is determined by reducing the weighted group variances, where the weight is indicated as probability of the individual groups $p(i)$. The probability of the groups $p(i)$ is calculated using Eq. (13).

$$p(i) = \frac{number\ \{(r,c)|image(r,c)=i\}}{(R,C)} \quad (13)$$

Where, r is represented as row of the fundus image, c is indicated as column of the image, C and R are stated as number of columns and rows of the image. The mean $\mu_b(t)$, weight, $w_b(t)$and variance $\sigma_b^2(t)$ of the class $T0$ are calculated using the Eqs. (14) - (16).

$$\mu_b(t) = \frac{\sum_{i=1}^{t} i \times p(i)}{w_b(t)} \quad (14)$$

$$w_b(t) = \sum_{i=1}^{t} p(i) \quad (15)$$

$$\sigma_b^2(t) = \frac{\sum_{i=1}^{t} (i-\mu_b(t))^2 \times p(i)}{w_b(t)} \quad (16)$$

Correspondingly, the mean, weight and variance of the class $T1$ are estimated by using the Eq. (17) - (19).

$$\mu_f(t) = \frac{\sum_{i=t+1}^{l} i \times p(i)}{w_f(t)} \quad (17)$$

$$w_f(t) = \sum_{i=t+1}^{l} p(i) \quad (18)$$

$$\sigma_f^2(t) = \frac{\sum_{i=t+1}^{l} (i-\mu_f(t))^2 \times p(i)}{w_f(t)} \quad (19)$$

At last, the best threshold value t^* is obtained with minimum within class variance σ_w^2 as mentioned in Eq. (20). After applying Otsu thresholding, the morphological transform related to vessel shape and size distribution is used for resizing the shape and size of the non microaneurysms and microaneurysms candidates.

$$\sigma_w^2 = w_b(t) \times \sigma_b^2(t) + w_f(t) \times \sigma_f^2(t) \quad (20)$$

3.4 Optimization using grey wolf optimization (GWO)

After vessel removal, GWO is used to predict the correctness of segmented microaneurysms candidates. GWO is a metaheuristic model that imitates the social hierarchy and hunting behaviour of grey wolves. The undertaken model works based on the three steps encircling, hunting and attacking prey. For modelling the hierarchy of wolves, consider the best solution namely alpha and the second and third best solutions are named as beta and delta respectively. Additionally, the remaining solutions are considered as omega. Initially, the grey wolf encircles the prey during the hunt. Encircling

Figure. 6 Output of template matching

performance of grey wolves is simulated using the Eqs. (21) and (22).

$$D = \left|C.X_{prey}(t) - X_{wolf}(t)\right| \quad (21)$$

$$X_{wolf}(t+1) = X_{prey}(t) - A.D \quad (22)$$

Where, t is indicated as current iteration, X_{prey} is represented as position of prey, A and C are represented as coefficient vectors, and X_{wolf} is indicated as position of grey wolf. The vectors A and C are determined by using the Eqs. (23) and (24).

$$A = 2\vec{a}.\vec{r}_1 - \vec{a}, \quad (23)$$

$$C = 2\vec{r}_2 \quad (24)$$

Where, $\vec{a}$ is decreased from two to zero over the course of iterations and $\vec{r}_1$ and $\vec{r}_2$ are denoted as random values$[0,1]$. Usually, the hunt is guided by alpha value, where occasionally beta and delta values are also participating to guide the hunt. For imitating the hunting behaviour of grey wolves, three best solutions of alpha, beta and delta values are obtained. Other search agents like omega updates their position based on the Eqs. (25) - (27). The blood vessel enhanced and segmented images are graphically presented in Fig. 5.

$$D_{alpha} = \left|C_1.X_{alpha} - X\right|, D_{beta} = |C_2.X_{beta} - X|, D_{delta} = |C_2.X_{delta} - X| \quad (25)$$

$$X_1 = X_{alpha} - A_1.D_{alpha}, X_2 = X_{beta} - A_2.D_{beta}, X_3 = X_{delta} - A_3.D_{delta} \quad (26)$$

$$X(t+1) = \frac{\vec{X}_1 + \vec{X}_2 + \vec{X}_3}{3} \quad (27)$$

3.5 Template matching

After segmenting the microaneurysms and non-microaneurysms regions, template matching is used to find the small parts of an image, which match a template image.

Template matching is utilized as a part of quality control. Fig 6 represents the output of template matching.

4. Results and discussion

This section presents a detailed discussion about the experimental result and discussion of the proposed model. In this study, MATLAB (version 2018A) is utilized for simulations in Personal Computer consists of 8 GB RAM, 3.0 GHz Intel i5 processor and one TB hard disc. The performance of the proposed model is compared with some previous research models; FCNN [1], Local Convergence Index (LCI) features [13], local features with K-Nearest Neighbour (KNN) Classifier [14] and DLC [21] on the E-ophtha and DiaretDB1 databases in terms of sensitivity against FPI, AUC, f-score, and accuracy to estimate efficacy of the proposed model. The performance measure is determined as the procedure of investigating, collecting and reporting the information based on system performance. Mathematical equation of f-score and accuracy are denoted in the Eqs. (28) and (29).

$$F - score = \frac{2TP}{2TP+FP+FN} \quad (28)$$

$$Accuracy = \frac{TN+TP}{TN+TP+FN+FP} \times 100 \quad (29)$$

where, TP is represented as true positive, TN is indicated as true negative, FP is indicated as false positive, and FN is indicated as false negative. Additionally, AUC measures the whole 2D area underneath the entire ROC curve from $(0,0)$ to $(1,1)$. In addition, Free Response Operating Characteristic Curve (FROC) is used to measure the performance of Microaneurysms detection by plotting sensitivity against the average number of FPI.

The sensitivity states the proportion of Microaneurysms candidate correctly detected by the proposed model, while FPI is the number of non-Microaneurysms candidate wrongly detected. For comparing the performance of existing and proposed model, the sensitivity values for the FPI rate values of 1/8, ¼, ½, 1, 2, 4, and 8 are obtained from the FROC curve. The AUC is graphically presented in Fig. 7.

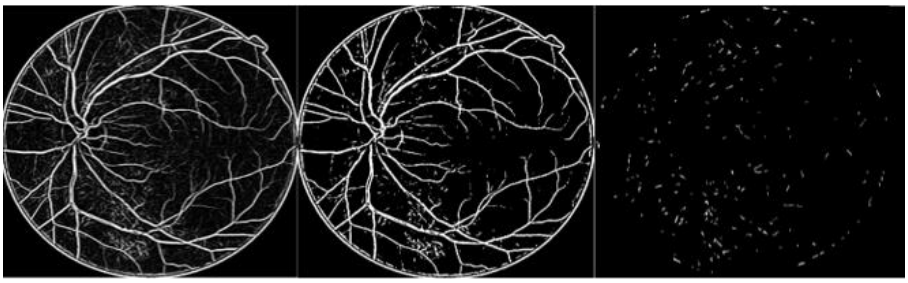

(a) (b) (c)

Figure. 5 Enhanced and optimized images: (a) hessian based filter output, (b) otsu threshold binary vasculature, and (c) GWO optimized image

Table 1. Performance evaluation of the proposed model on E-ophtha database

Method	Sensitivity against FPI							F-Score	AUC	Accuracy (%)
	1/8	1/4	½	1	2	4	8			
LCI features[13]	0.358	0.417	0.471	0.522	0.558	0.605	0.638	0.51	0.575	-
Local features with KNN [14]	0.063	0.117	0.172	0.245	0.323	0.417	0.573	0.273	0.386	-
DLC [21]	0.075	0.075	0.267	0.358	0.472	0.594	0.69	0.374	-	-
Proposed model	**0.361**	**0.495**	**0.591**	**0.58**	**0.61**	**0.72**	**0.69**	**0.5781**	**0.6796**	**85.72**

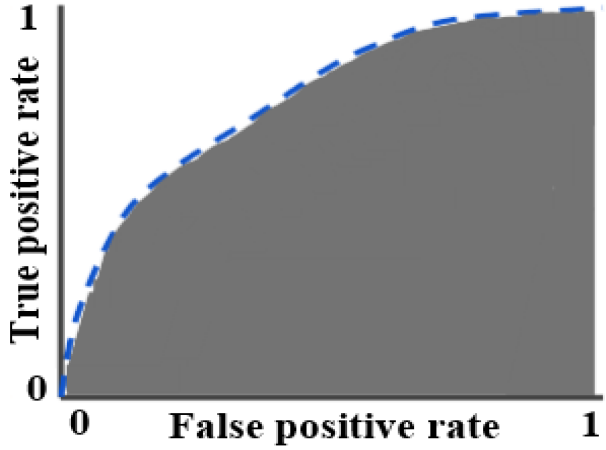

Figure. 7 Graphical depiction of AUC

4.1 Quantitative analysis on E-ophtha dataset

The E-ophtha database is used to analyze the performance of the proposed model. The Table 1 presents the performance of the proposed model in terms of sensitivity against FPI, AUC, f-score, and accuracy. The performance evaluation is validated for one sample fundus image in the E-ophtha database. For the collected image, f-score of the proposed technique is 0.5781 and the existing models LCI features [13], local features with KNN Classifier [14], and DLC [21] delivers 0.51, 0.273 and 0.374 of f-score. In addition, AUC of the proposed technique is 0.6796 and the existing methodologies delivers 0.575 and 0.386 of AUC. Correspondingly, the sensitivity against FPI of the proposed model is better compared to other comparative models in the all seven circumstances. In the E-ophtha database, the proposed model delivers 85.72% of accuracy. The comparison of the proposed and existing models on E-ophtha database is graphically presented in the Fig. 8 and 9.

4.2 Quantitative analysis on DiaretDB1 dataset

In this section, DiaretDB1 database is used to analyse the performance of the proposed model. The Table 2 presents the performance valuation of one sample image in DiaretDB1 dataset. For the collected fundus image, f-score of the proposed technique is 0.610 and the existing works; FCNN [1], LCI features [13] and DLC [21] delivers 0.392, 0.547 and 0.210 of f-score. In addition, the AUC of the proposed technique is 0.725 and the existing LCI features [13] delivers 0.565 of AUC. The results indicate that the sensitivity against FPI of the proposed model is superior compared to other comparative work in the all seven conditions; 1/8, ¼, ½, 1, 2, 4, and 8.

In addition, the proposed model delivers 86.16% of accuracy in DiaretDB1 database. The Tables 1 and 2 reveal that the proposed model performs well in microaneurysms detection compared to the conventional methods. In this study, optimization is a key part of microaneurysms detection where GWO selects the microaneurysms candidates from the non-microaneurysms candidates that is graphically presented in the Fig. 5. The comparison between the proposed and existing method on DiaretDB1 database is represented in the Fig. 10 and 11.

Table 2. Performance evaluation of the proposed model on DiaretDB1 database

Method	Sensitivity against FPI							F-Score	AUC	Accuracy (%)
	1/8	1/4	½	1	2	4	8			
LCI features [13]	0.507	0.517	0.519	0.53	0.555	0.574	0.617	0.547	0.565	-
DLC [21]	0.013	0.026	0.052	0.104	0.209	0.400	0.669	0.210	-	-
FCNN [1]	0.187	0.246	0.288	0.365	0.449	0.570	0.641	0.392	-	-
Proposed model	**0.570**	**0.551**	**0.601**	**0.612**	**0.621**	**0.631**	**0.690**	**0.610**	**0.725**	**86.16**

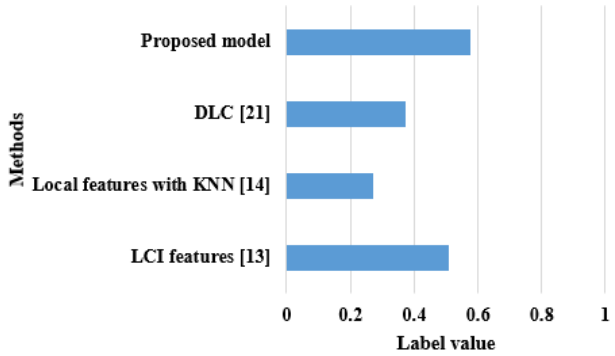

Figure. 8 Comparison between the proposed and existing methods on E-ophtha database in terms of f-score

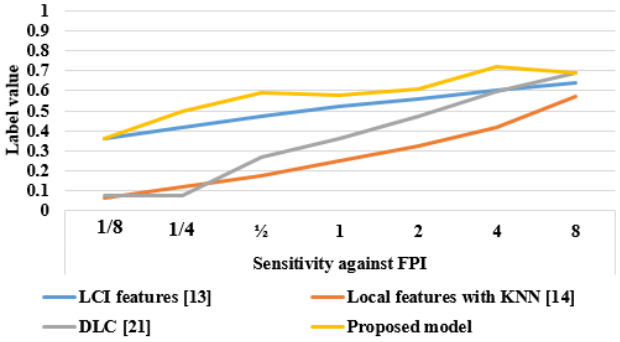

Figure. 9 Comparison between the proposed and existing methods on E-ophtha database in terms of sensitivity against FPI

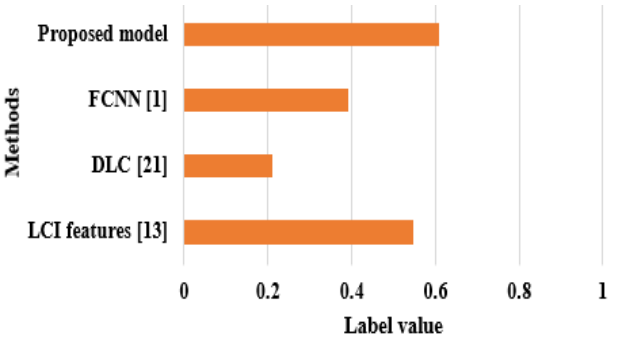

Figure. 10 Comparison between the proposed and existing methods on DiaretDB1 database in light of f-score

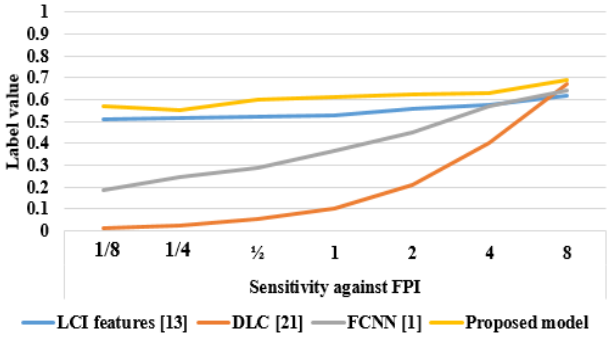

Figure. 11 Comparison between the proposed and existing methods on DiaretDB1 database in light of sensitivity against FPI

5. Conclusion

In this paper, an automated model was proposed for accurate detection of microaneurysms using retinal fundus image. In the first stage, normalization, gradient weighting, shade correction and low light image enhancement were accomplished to enhance the visibility of the retinal fundus images. Next, Hessian based filter and Otsu thresholding were used to extract the foreground objects blood vessels, microaneurysms, etc. from the fundus images. At last, GWO was utilized to select only the microaneurysms candidates from the images. The proposed automated model delivered better performance in terms of sensitivity against FPI, AUC, f-score and accuracy compared to the existing models LCI features and local features with KNN Classifier. The experimental results revealed that the proposed model achieved 0.06-0.30 improvement in f-score compared to the existing methods on E-ophtha microaneurysms and DiaretDB1 datasets. Additionally, the proposed model achieved 85.72% and 86.16% of segmentation accuracy on e-ophtha microaneurysms and DiaretDB1 datasets respectively. In future work, a new deep learning classifier can be included in the proposed model to classify both the microaneurysms and non-microaneurysms candidates from the images.

Conflicts of Interest

The authors declare no conflict of interest.

Author Contributions

The paper conceptualization, methodology, software, validation, formal analysis, investigation, resources, data curation, writing—original draft preparation, writing—review and editing, visualization, have been done by 1st author. The supervision and project administration, have been done by 2nd author.

References

[1] P. Chudzik, S. Majumdar, F. Calivá, B. Al-Diri, and A. Hunter, "Microaneurysm detection using fully convolutional neural networks", *Computer Methods and Programs in Biomedicine*, Vol. 158, pp. 185-192, 2018.

[2] B. Antal and A. Hajdu, "Improving microaneurysm detection in color fundus images by using context-aware approaches", *Computerized Medical Imaging and Graphics*, Vol. 37, No. 5-6, pp. 403-408, 2013.

[3] N. Eftekhari, H. R. Pourreza, M. Masoudi, K. Ghiasi-Shirazi, and E. Saeedi, "Microaneurysm detection in fundus images using a two-step convolutional neural network", *Biomedical Engineering Online*, Vol. 18, No. 1, pp. 67, 2019.

[4] S. S. Rahim, C. Jayne, V. Palade, and J. Shuttleworth, "Automatic detection of microaneurysms in colour fundus images for diabetic retinopathy screening", *Neural Computing and Applications*, Vol. 27, No. 5, pp. 1149-1164, 2016.

[5] W. Cao, N. Czarnek, J. Shan, and L. Li, "Microaneurysm detection using principal component analysis and machine learning methods", *IEEE Transactions on Nanobioscience*, Vol. 17, No. 3, pp. 191-198, 2018.

[6] M. U. Akram, S. Khalid, and S. A. Khan, "Identification and classification of microaneurysms for early detection of diabetic retinopathy", *Pattern Recognition*, Vol. 46, No. 1, pp. 107-116, 2013.

[7] B. Antal, and A. Hajdu, "Improving microaneurysm detection using an optimally selected subset of candidate extractors and preprocessing methods", *Pattern Recognition*, Vol.45, No.1, pp.264-270, 2012.

[8] B. Zhang, F. Karray, Q. Li, and L. Zhang, "Sparse representation classifier for microaneurysm detection and retinal blood vessel extraction", *Information Sciences*, Vol. 200, pp. 78-90, 2012.

[9] S. Jiménez, P. Alemany, F. J. Núñez, I. Fondón, C. Serrano, B. Acha, and I. Failde, "Automated detection of microaneurysms by using region growing and fuzzy artmap neural network", *Archivos de la Sociedad Española de Oftalmología (English Edition*), Vol. 87, No. 9, pp. 284-289, 2012.

[10] P. Khojasteh, B. Aliahmad, and D. K. Kumar, "Fundus images analysis using deep features for detection of exudates, hemorrhages and microaneurysms", *BMC Ophthalmology*, Vol. 18, No. 1, pp .288, 2018.

[11] T. Selçuk and A. Alkan, "Detection of Microaneurysms using ant colony algorithm in early diagnosis of diabetic retinopathy", *Medical Hypotheses*, Vol. 129, pp. 109242, 2019.

[12] J. Xu, X. Zhang, H. Chen, J. Li, J. Zhang, L. Shao, and G. Wang, "Automatic analysis of microaneurysms turnover to diagnose the progression of diabetic retinopathy", *IEEE Access*, Vol. 6, pp. 9632-9642, 2018.

[13] B. Dashtbozorg, J. Zhang, F. Huang, and B.M. ter Haar Romeny, "Retinal microaneurysms detection using local convergence index features", *IEEE Transactions on Image Processing*, Vol. 27, No. 7, pp. 3300-3315, 2018.

[14] B. Wu, W. Zhu, F. Shi, S. Zhu, and X. Chen, "Automatic detection of microaneurysms in retinal fundus images", *Computerized Medical Imaging and Graphics*, Vol. 55, pp. 106-112, 2017.

[15] R. Rosas-Romero, J. Martínez-Carballido, J. Hernández-Capistrán, and L. J. Uribe-Valencia, "A method to assist in the diagnosis of early diabetic retinopathy: Image processing applied to detection of microaneurysms in fundus images", *Computerized Medical Imaging and Graphics*, Vol. 44, pp. 41-53, 2015.

[16] E. Decencière, G. Cazuguel, X. Zhang, G. Thibault, J. C. Klein, F. Meyer, B. Marcotegui, G. Quellec, M. Lamard, R. Danno, and D. Elie, "TeleOphta: Machine learning and image processing methods for teleophthalmology", *IRBM*, Vol. 34, No. 2, pp. 196-203, 2013.

[17] X. Dong, G. Wang, Y. Pang, W. Li, J. Wen, W. Meng, and Y. Lu, "Fast efficient algorithm for enhancement of low lighting video", In: *Proc. of IEEE International Conf. on Multimedia and Expo*, pp. 1-6, 2011.

[18] C. C. Reyes-Aldasoro, "Retrospective shading correction algorithm based on signal envelope estimation", *Electronics letters*, Vol. 45, No. 9, pp. 454-456, 2009.

[19] I. Usman, and K. A. Almejalli, "Intelligent Automated Detection of Microaneurysms in Fundus Images Using Feature-Set Tuning", *IEEE Access*, Vol. 8, pp. 65187-65196, 2020.

[20] S. B. Patil and B. P. Patil, "Automatic Detection of Microaneurysms in Retinal Fundus Images using Modified High Boost Filtering, Line Detectors and OC-SVM", In: *Proc. of the International Conf. on Industry 4.0 Technology (I4Tech)*, pp. 148-153, 2020.
[21] S. Long, J. Chen, A. Hu, H. Liu, Z. Chen, and D. Zheng, "Microaneurysms detection in color fundus images using machine learning based on directional local contrast", *BioMedical Engineering OnLine*, Vol. 19, pp. 1-23, 2020.
[22] E-ophtha dataset link: http://www.adcis.net/en/third-party/e-ophtha/
[23] DiaretDB1 dataset link: https://www.it.lut.fi/project/imageret/diaretdb1_v2_1/